Electronic Supplementary Information

# (Plasmonic gold core)@(ultrathin ruthenium shell) nanostructures as antenna-reactor photocatalysts toward nitrogen photofixation

Henglei Jia,[#] Yuanyuan Yang,[#] Yanrong Dou, Fan Li, Mengxuan Zhao and Chun-yang Zhang*

College of Chemistry, Chemical Engineering and Materials Science, Shandong Normal University, Jinan 250014, China

* Corresponding author. E-mail: cyzhang@sdnu.edu.cn

[#] These authors contributed equally to this work.

**Supporting Experimental Section**

**Chemicals.** Polyvinylpyrrolidone (PVP, MW = 55,000), sodium borohydride ($NaBH_4$, 99%), silver nitrate ($AgNO_3$, ≥ 99.0%), L-Ascorbic acid (AA, ≥ 99%), methanol ($CH_3OH$, ≥ 99.9%) were purchased from Sigma-Aldrich. Tetrachloroauric (III) acid tetrahydrate ($HAuCl_4{\cdot}4H_2O$), hydrochloric acid (HCl, 36.0 – 38.0 w%), sodium hydroxide (NaOH, ≥ 96%) were obtained from Sinopharm Chemical Reagent. Cetyltrimethylammonium bromide (CTAB, > 98%) was obtained from Alfa Aesar. Ruthenium chloride hydrate ($RuCl_3{\cdot}xH_2O$, 35 – 42% Ru) and salicylic acid ($C_6H_4(OH)COOH$, ≥ 99.0%) were purchased from Aladdin Reagent. Sodium nitroferricyanide (III) dihydrate ($Na_2[Fe(CN)_5NO]{\cdot}2H_2O$, 99%) was purchased from Macklin. Nitrogen ($^{14}N_2$, 99.999%), nitrogen ($^{15}N_2$, 98 atom% $^{15}N$), and argon (Ar, 99.999%) were used as received. Deionized (DI) water with a resistivity of 18.2 MΩ·cm was used in all experiments.

**Growth of Au NRs.** The Au NRs were prepared by using a seed-mediated growth method with slightly modifications.[1,2] Specifically, the seed solution was prepared by adding a freshly prepared ice-cold $NaBH_4$ solution (0.01 M, 0.6 mL) into a mixture containing CTAB (0.1 M, 9.75 mL) and $HAuCl_4$ (0.01 M, 0.25 mL). The resultant solution was mixed by rapid inversion for 2 min and then keeping at room temperature for 2 h prior to use. The growth solution was made by sequential addition of $HAuCl_4$ (0.01 M, 2 mL), $AgNO_3$ (0.01 M, 0.4 mL), HCl (1 M, 0.8 mL), and AA (0.1 M, 0.32 mL) into CTAB solution (0.1 M, 40 mL), followd by the injection of seed solution (10 μL) into the growth solution. The resultant solution was mixed by rapid inversion for 2 min and kept undisturbed for at least 6 h.

**Preparation of Au NR@Ru NCs.** The Au NR@Ru NCs were prepared by the overgrowth of urtrathin Ru shell on pre-grown Au NR core through a seed-mediated growth method. Typically, the as-prepared Au NR solution (optical density at the longitudinal plasmon wavelength = 2.0, 5 mL) was centrifuged at 5000 rpm for 10 min and then washed with DI water (5 mL) to remove the excess surfactant. The precipitate was redispersed in CTAB solution (0.1 M, 125 μL) to obtain a final CTAB concentration of 1.25 mM. For the growth of ultrathin Ru shell, DI water (5.075 mL), PVP solution (MW = 55000, 50 $mg{\cdot}mL^{-1}$, 4 mL), and $RuCl_3$ solution (0.1 M, 100 μL) were added into the Au NR solution. The resultant solution was mixed by reversion for 10 s, followd by the addition of a freshely prepared ice-cold $NaBH_4$ solution (0.1 M, 200 μL). The resultant solution was mixed by inversion for 10 s and kept in an oven setted at 80 °C for 2 h.

**Preparation of Ru nanocrystals.** The preparation method of Ru nanocrystals was similar to that of the Au NR@Ru NCs. Specifically, the Ru nanocrystals were prepared by sequential addition of CTAB (0.1 M, 25 μL), $RuCl_3$ (0.1 M, 100 μL), and PVP (MW = 55000, 50 mg/mL) into DI water (3.65 mL). The resultant solution was mixed by inversion for 10 s, followd by the addition of a freshely prepared ice-cold $NaBH_4$ solution (0.1 M, 200 μL). The resultant solution was mixed by inversion for 10 s and kept in an oven setted at 80 °C for 2 h.

**Nitrogen photofixtion reaction.** The $N_2$ photofixation reaction was conducted in a customized three-necked reactor with three ends. Two side ends were employed as inlet and outlet for gas flow, while the middle end was equipped with a quartz window on the top for light illumination. For a typical photocatalytic process, the photocatalyst (0.5 mg) was dispersed into DI water (8 mL). $CH_3OH$ (2 mL) was added and employed as the hole scavenger. The resultant mixture solution was bubbled with high-purity $N_2$ (30 $mL \cdot min^{-1}$) at a pressure of 1 atm for 10 min. A continuous Xe lamp (300 W) equipped with an AM 1.5G filter and a 420 nm cutoff filter was employed as the light source for illumination. The optical power density was 400 $mW \cdot cm^{-2}$. The reaction temperature was kept at 25 °C using a circulation cooling system. The photocatalytic reaction was carried out under the light irradiation ($\lambda > 420$ nm) for 2 h. For each 30 min, an aliquot of the reaction solution (0.75 mL) was taken out, and the catalyst was removed by centrifugation. The concentration of the produced ammonia in the supernatant was quantitatively analyzed with the indophenol-blue method.[3,4] The action spectrum was acquired by perfoming the photocatalytic $N_2$ fixation under the irradiation of different monochromatic light by using an additional bandpass filter (600, 650, 670, 700, 730, 765, and 808 nm) in the typical photocatalytic process. The optical power density was setted at 50 $mW \cdot cm^{-2}$ for the action spectrum measurement. All the full widths at half-maximum of the bandpass filters are all 20 nm. The turnover number (TON) for the $NH_3$ production was calculated as the molar ratio of the $NH_3$ production amount to the Ru atoms in the Au NR@Ru NCs. The turnover frequency (TOF) was determined as the TON per unit time.

**Growth mechanism of Ru nanocluster shell on Au NRs.** The Au NR@Ru NCs were prepared through the growth of Ru nanocluster shell on the pre-grown Au NRs. The pre-grown Au NRs that were stabilized with CTAB bilayers were employed as the cores.[1,2] For the growth of Ru nanocluster shell, $RuCl_3$, $NaBH_4$, and

PVP were used as the precursor, the reducing agent, and the surfactant, respectively. Ru nanoclusters were formed by the reduction of $RuCl_3$ with $NaBH_4$ at a temperature of 80 °C, with the protection of surfactant molecules. At a low CTAB concentration (< 0.75 mM), the CTAB bilayers on the Au NRs were packed less compact. Ru nanoclusters stabilized with PVP were readily coated on the Au NR surface to form a Ru nanocluster shell. Owing to the larger curvature at the ends than that on the side of the Au NRs,[5] Ru nanoclusters preferentially nucleated at the ends of Au NRs (Fig. 1d). With the increase of CTAB concentration (0.75–2 mM), the surface of Au NRs was densely covered by the surfactant molecules, which blocked the coating of Ru nanoclusters and decreased the Ru shell thickness. Since the surface of Au NRs were densely covered by CTAB molecules, the further increase of CTAB concentration (> 2 mM) affected less on the Ru shell thickness. Therefore, the thickness of ultrathin Ru nanocluster shell can be readily varied by changing the CTAB concentration.

**Characterization.** TEM imaging was conducted on an HT7700 electron microscope. HRTEM, HAADF-STEM imaging and EDX mapping were performed on a FEI Themis Z microscopy. The extinction spectra were recorded using a Hitachi U-3900 ultraviolet/visible/NIR spectrophotometer. XRD patterns were arried out on a Smart Lab Se diffractometer equipped with Cu Kα radiation. XPS spectra were obtained on a Thermo Scientific ESCALAB 250Xi spectrometer. Inductively coupled plasma optical emission spectroscopy (ICP-OES) was conducted on a PerkinElmer Optima 7300 DV system. $^1$H NMR spectra were measured on a Bruker Avance III HD 600 NMR spectrometer.

**Supplementary Figures**

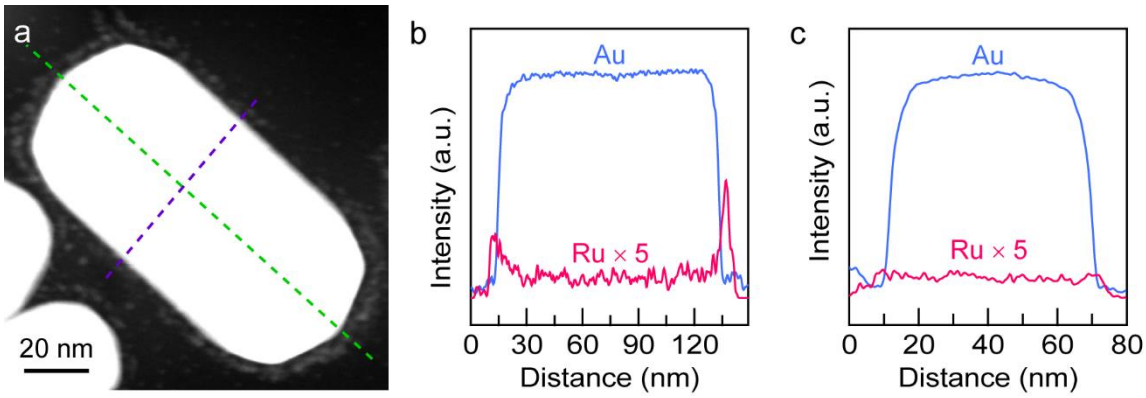


**Fig. S1.** Elemental profiles of a single Au NR@Ru NC. (a) HAADF-STEM image. (b and c) Elemental maps of Au and Ru acquired along the dashed green (b) and purple (c) lines indicated in (a).

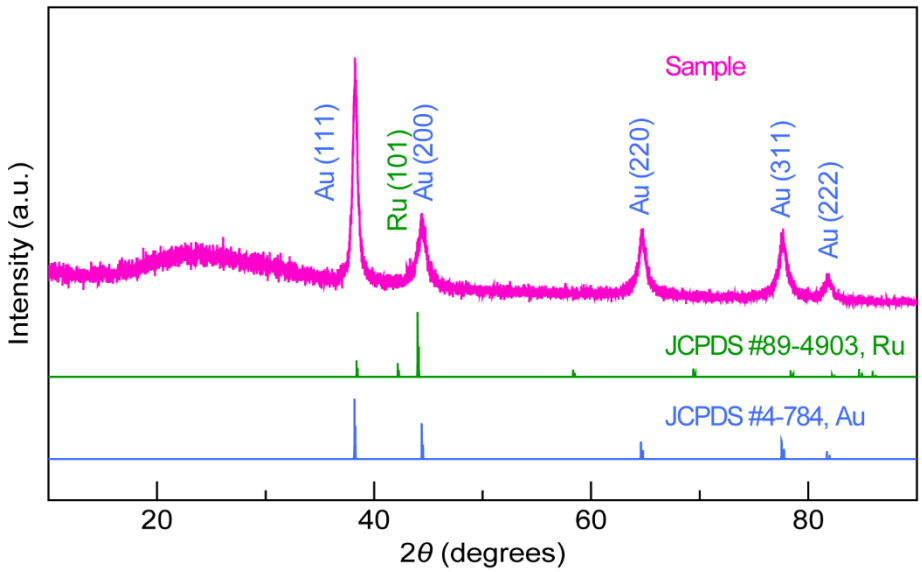


**Fig. S2.** XRD patterns of a representative Au NR@Ru NC sample. The blue and green curves are the standard powder diffraction patterns of the face-centered-cubic structure of Au (space group, F*m*-3*m*; lattice constant, 0.40786 nm) and the hexagonal structure of Ru (space group, P63/mmc; lattice constant, 0.27058 nm).

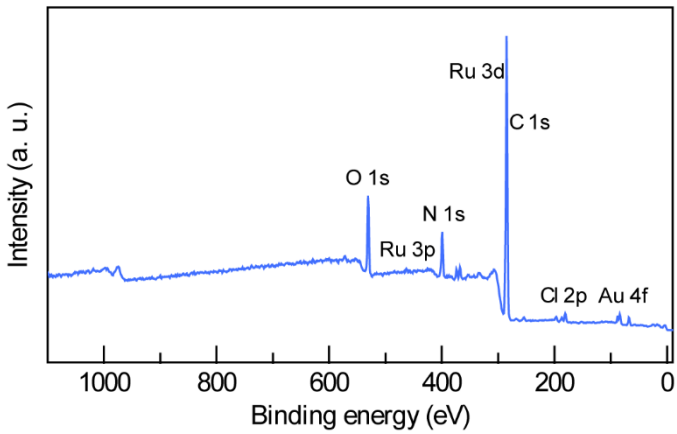


**Fig. S3.** XPS survey spectrum of a representative Au NR@Ru NC sample.

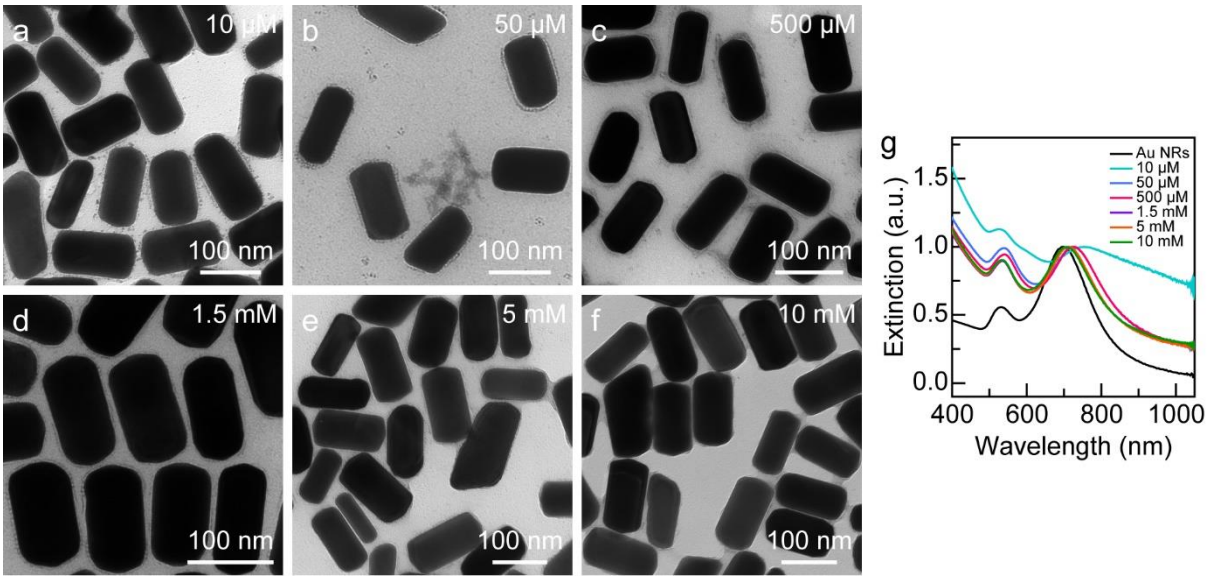


**Fig. S4.** Representative TEM images of the Au NR@Ru NCs when the CTAB concentration was 10 μM (a), 50 μM (b), 500 μM (c), 1.5 mM (d), 5 mM (e), and 10 mM (f), respectively. (g) Extinction spectra of the Au NR@Ru NCs obtained when different CTAB concentrations were employed for the Ru shell overgrowth.

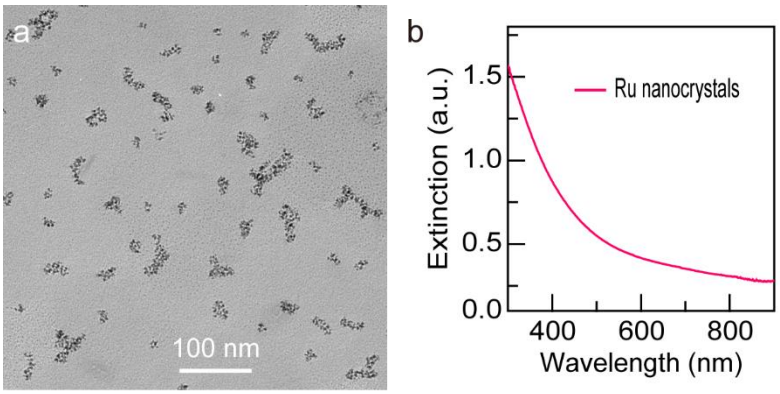


**Fig. S5.** TEM image (a) and extinction spectrum (b) of the Ru nanocrystals used for the $N_2$ photofixation.

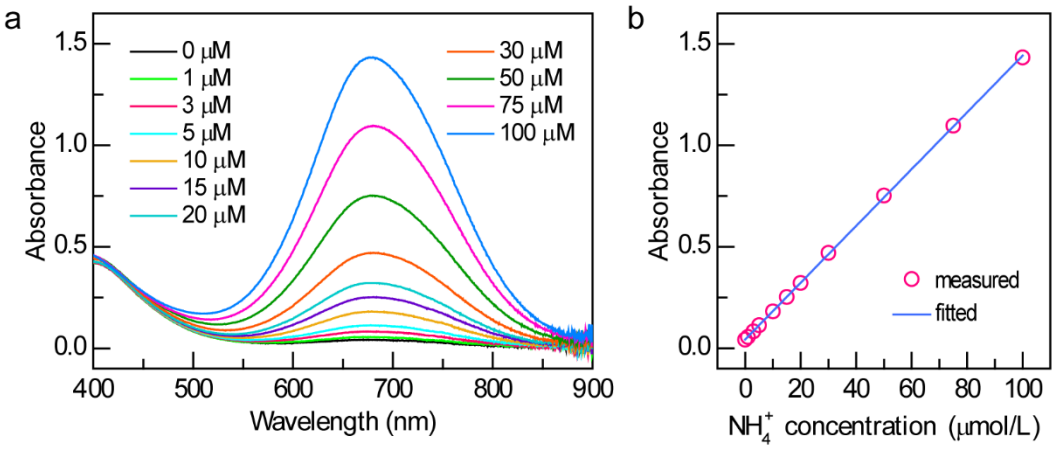


**Fig. S6.** (a) Absorption spectra of the standard $NH_4^+$ solutions at different concentrations. (b) Linear relationship between the absorbance value and the standard $NH_4^+$ solution concentration. The coefficient of determination for the linear fitting is $R^2 = 0.99987$.

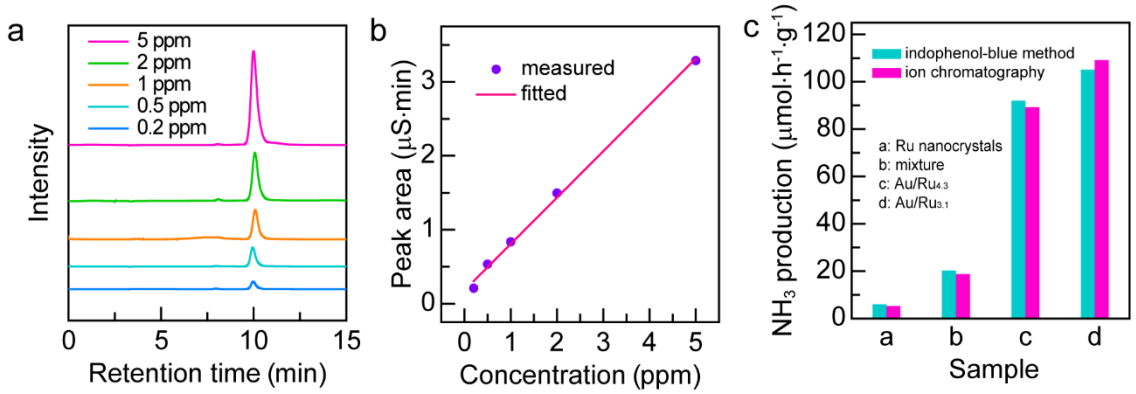


**Fig. S7.** (a) Ion chromatography spectra of the standard $NH_4^+$ solutions with different concentrations. (b) Linear relationship between the peak area values and the standard $NH_4^+$ solution concentration. The coefficient of determination for the linear fitting is $R^2$ = 0.99635. (c) Comparison of the $NH_3$ production rates on different catalysts determined using two different detection methods.

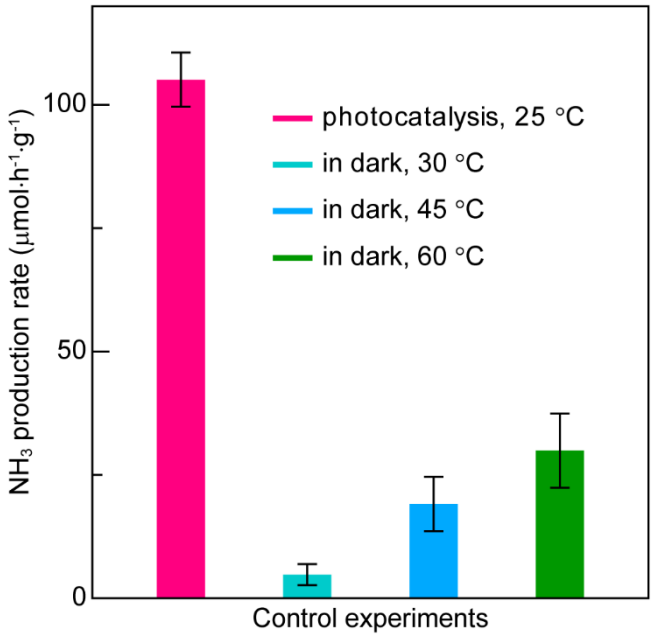


**Fig. S8.** $N_2$ reduction experiments performed under different conditions.

To prevent the increasing temperature of the reaction solution caused by the photothermal effect of plasmonic Au NRs, the solution temperature was kept at 25 °C using a circulation cooling system. In addition, the solution temperature is 45 °C after 2-h irradiation in the absence of the circulation cooling system. To reveal the contribution of photothermal effect upon the photocatalysis, we carried out additional experiments by

performing the $N_2$ reduction reaction in water bathes set at different temperatures (30, 45, and 60 °C) in the dark (Fig. S8). The $N_2$ fixation activities conducted in water bathes are very low compared with that under the light irradiation, suggesting that the contribution of photothermal heating is small. Notably, this result suggests that the Au NR@Ru NCs can also work as a thermochemical catalyst in addition to the hot-electron source. It is generally accepted that there is a local temperature elevation nearby the plasmonic metal.[6,7] Since the reaction rate and apparent quantum efficiency increase with the operating temperature,[6] the photothermal heating effect can hardly be ruled out in this system. Therefore, thermal and plasmonic hot carriers are synergistic with each other and make contributions to the $N_2$ photofixation activities of the Au NR@Ru NCs.

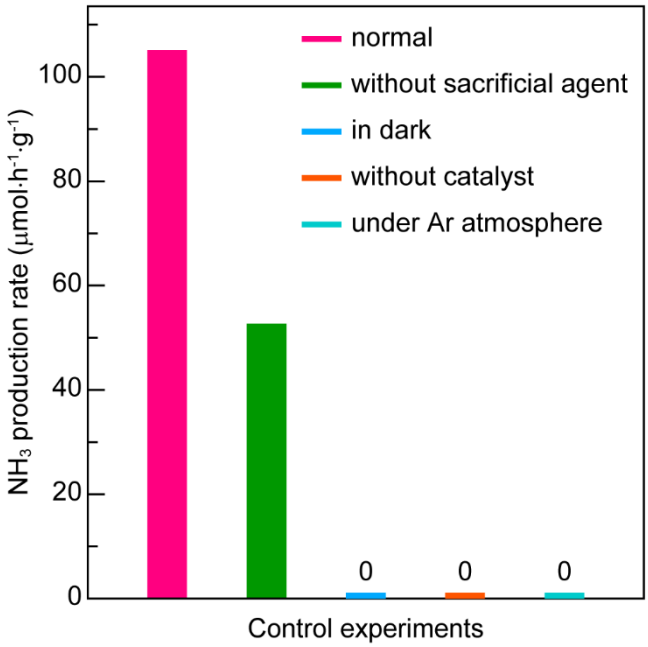


**Fig. S9.** Control experiments of the $N_2$ photofixation under different conditions.

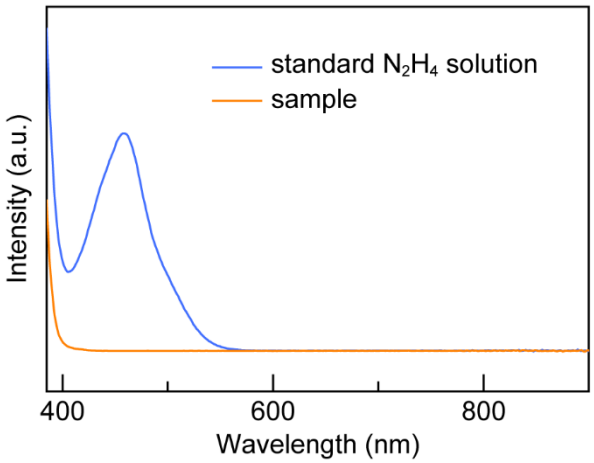


**Fig. S10.** Detection of the possible $N_2H_4$ byproduct.

It has been reported that other byproducts (e.g., $NO_3^-$ and $N_2H_4$) may be generated during $N_2$ photofixation through the oxidation of $NH_3$ by the generated holes or the reduction of $N_2$ by hot electrons, respectively.[8] We conducted additional experiments to examine the possible byproducts. The possible presence of oxidation product $NO_3^-$ was detected using ion chromatograph. No $NO_3^-$ is detected after 2-h typical photocatalytic process. In addition, the possible reduction byproduct $N_2H_4$ was measured using a spectrophotometric method.[9] As shown in Fig. S10, the byproduct $N_2H_4$ is not detected in the typical photocatalytic process. Neither $NO_3^-$ nor $N_2H_4$ is detected in the photocatalytic reaction, demonstrating the high selectivity of $N_2$ photofixation.

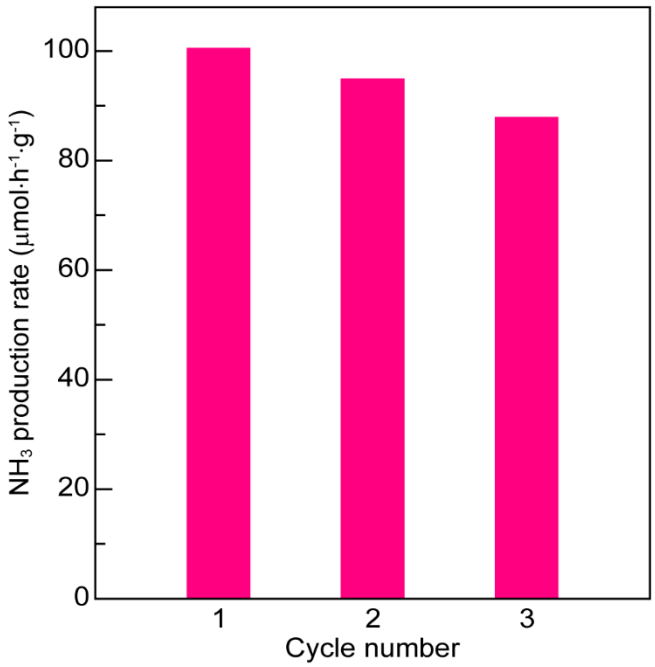


**Fig. S11.** $NH_3$ production rates of three successive cycles.

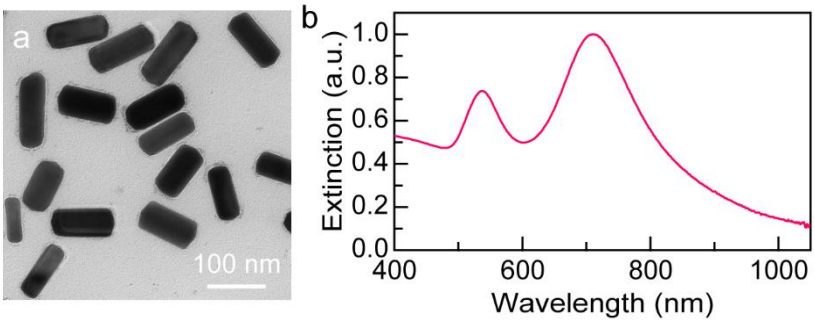


**Fig. S12.** TEM image (a) and extinction spectrum (b) of the Au NR@Ru NCs after 2-h $N_2$ photofixation.

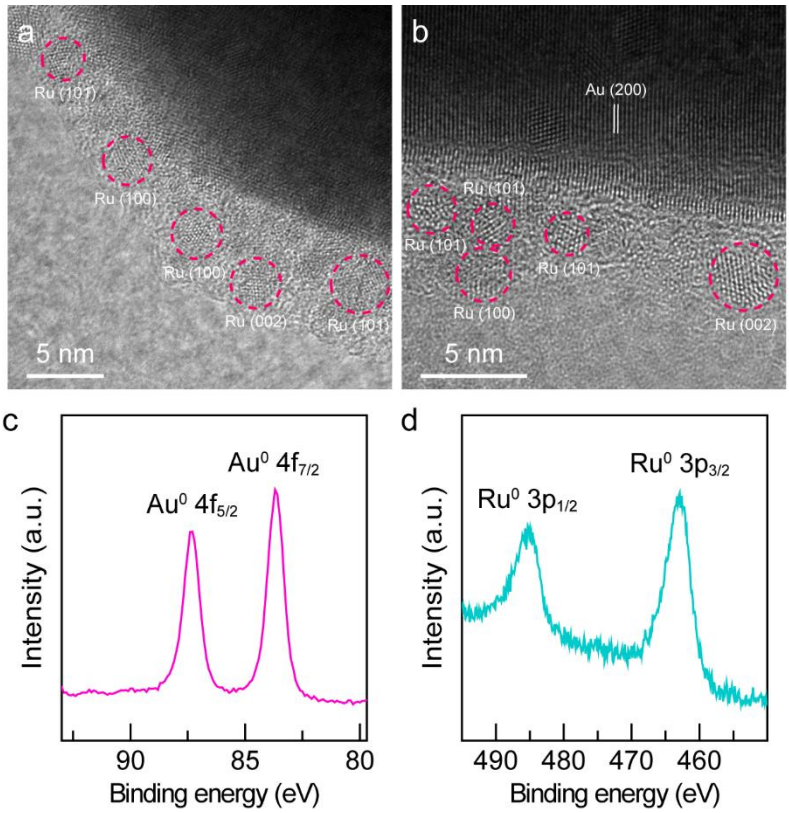


**Fig. S13.** Aberration-corrected HRTEM images of the Au–Ru interface at the end (a) and on the side surface (b) of the Au NR after the photocatalytic process. High-resolution Au 4f (c) and Ru 3p (d) spectra of the Au NR@Ru NCs after the typical photocatalytic reaction.

To examine the stability of Au NR@Ru NCs in the catalytic reaction, TEM image and extinction spectrum of the catalyst after 2-h $N_2$ photofixation reaction were obtained. As shown in Fig. S12, neither morphological nor plasmonic property changes is observed, suggesting the good stability of the catalyst. To further confirm the stability of catalyst in the catalytic reaction, aberration-corrected HRTEM imaging and XPS were performed (Fig. S13). Aberration-corrected HRTEM images taken at the Au–Ru interface clearly demonstrated that Ru nanoclusters remained nearly unchanged after the $N_2$ reduction reaction, indicating the excellent stability of the catalyst. In addition, XPS results confirmed that the valence states of Au and Ru in the catalyst remained unchanged after the catalytic reaction. Above all, our catalyst exhibited excellent stability in the $N_2$ photofixation reaction.

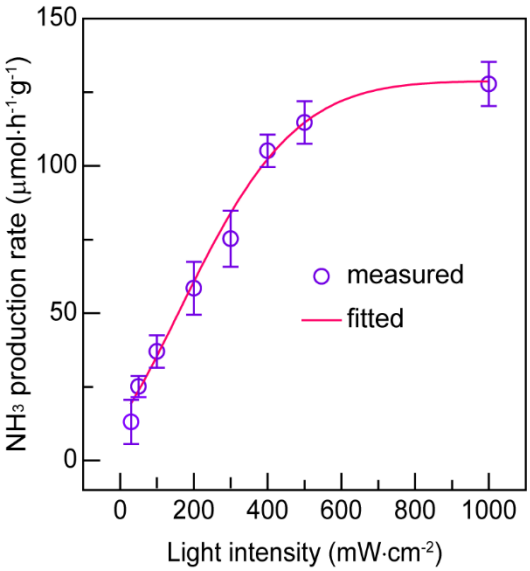


**Fig. S14.** Dependence of photocatalytic $NH_3$ generation rate upon the light intensity.

To investigate the dependence of the $N_2$ photofixation rate upon the photon flux, the photocatalytic experiments were conducted under different light intensities (30, 50, 100, 200, 300, 400, 500, and 1000 $mW{\cdot}cm^{-2}$). As shown in Figure S14, a nearly linear dependence of the $N_2$ reduction rate upon light intensity is observed when the light intensity is smaller than about 500 $mW{\cdot}cm^{-2}$. The slope of the curve for the $NH_3$ production rate against the light intensity become very small when the light intensity is further increased, suggesting the light intensity is saturation in this photocatalytic system. The linear activity−photon flux is an important indicator for the induction of a reaction by a single charge-carrier.[10,11] The linear dependence result reveals that the $N_2$ photofixation is driven by the plasmonic hot electrons. In addition, the absence of $N_2H_4$ in the photocatalytic system (Fig. S10) shows that the $N_2$ photofixation on Au NR@Ru NCs undergoes a dissociative mechanism rather than an associative alternating mechanism,[12] which has been reported in the AuRu core-antenna nanostructures.[13]

Based on the above results, a possible photocatalytic $N_2$ reduction mechanism on the Au NR@Ru NCs is proposed. Ru nanoclusters possess optimal $N_2$ adsorption energy that facilitates the adsorption and activation of $N_2$ molecules on their surface. Under the light irradiation, Au NRs harvest light and generate hot electrons and holes. The hot electrons transfer to the active sites on Ru nanoclusters, where the activated $N_2$ molecules are reduced by one hot electron and turned to charged state. $N_2$ molecules are further reduced to $NH_3$

following a dissociative mechanism, which is promoted by the local electric field enhancement caused by LSPR property of Au NRs.[13] Meanwhile, the hot holes are consumed by the hole sacrificial agent on Au NRs, achieving effective electron–hole separation.

**References**


1. B. Nikoobakht and M. A. El-Sayed, *Chem. Mater.*, 2003, **15**, 1957–1962.
2. W. H. Ni, X. S. Kou, Z. Yang and J. F. Wang, *ACS Nano*, 2008, **2**, 677–686.
3. J. H. Yang, Y. Z. Guo, R. B. Jiang, F. Qin, H. Zhang, W. Z. Lu, J. F. Wang and J. C. Yu, *J. Am. Chem. Soc.*, 2018, **140**, 8497–8508.
4. D. Zhu, L. H. Zhang, R. E. Ruther and R. J. Hamers, *Nat. Mater.*, 2013, **12**, 836–841.
5. H. L. Jia, A. X. Du, H. Zhang, J. H. Yang, R. B. Jiang, J. F. Wang and C.-Y. Zhang, *J. Am. Chem. Soc.*, 2019, **141**, 5083–5086.
6. P. Christopher, H. L. Xin, A. Marimuthu and S. Linic, *Nat. Mater.*, 2012, **11**, 1044–1050.
7. F. Wang, C. H. Li, H. J. Chen, R. B. Jiang, L.-D. Sun, Q. Li, J. F. Wang, J. C. Yu and C.-H. Yan, *J. Am. Chem. Soc.*, 2013, **135**, 5588–5601.
8. O. Rusina, O. Linnik, A. Eremenko and H. Kisch, *Chem. Eur. J.*, 2003, **9**, 561–565.
9. H. Li, J. Shang, Z. H. Ai and L. Z. Zhang, *J. Am. Chem. Soc.*, 2015, **137**, 6393–6399.
10. P. Christopher, H. L. Xin and S. Linic, *Nat. Chem.*, 2011, **3**, 467–472.
11. S. Mukherjee, F. Libisch, N. Large, O. Neumann, L. V. Brown, J. Cheng, J. B. Lassiter, E. A. Carter, P. Nordlander and N. J. Halas, *Nano Lett.*, 2013, **13**, 240–247.
12. M. A. Shipman and M. D. Symes, *Catal. Today*, 2017, **286**, 57–68.
13. C. Y. Hu, X. Chen, J. B. Jin, Y. Han, S. M. Chen, H. X. Ju, J. Cai, Y. R. Qiu, C. Gao, C. M. Wang, Z. M. Qi, R. Long, L. Song, Z. Liu and Y. J. Xiong, *J. Am. Chem. Soc.*, 2019, **141**, 7807–7814.